

Floquet-Enhanced Spin Swaps

Haifeng Qiao,¹ Yadav P. Kandel,¹ John S. Van Dyke,² Saeed Fallahi,^{3,4} Geoffrey C. Gardner,^{4,5} Michael J. Manfra,^{3,4,5,6} Edwin Barnes,² and John M. Nichol^{1,*}

¹*Department of Physics and Astronomy, University of Rochester, Rochester, NY, 14627 USA*

²*Department of Physics, Virginia Tech, Blacksburg, Virginia, 24061, USA*

³*Department of Physics and Astronomy, Purdue University, West Lafayette, IN, 47907 USA*

⁴*Birck Nanotechnology Center, Purdue University, West Lafayette, IN, 47907 USA*

⁵*School of Materials Engineering, Purdue University, West Lafayette, IN, 47907 USA*

⁶*School of Electrical and Computer Engineering,
Purdue University, West Lafayette, IN, 47907 USA*

The transfer of information between quantum systems is essential for quantum communication and computation. In quantum computers, high connectivity between qubits can improve the efficiency of algorithms, assist in error correction, and enable high-fidelity readout. However, as with all quantum gates, operations to transfer information between qubits can suffer from errors associated with spurious interactions and disorder between qubits, among other things. Here, we harness interactions and disorder between qubits to boost the fidelity of a swap operation for spin eigenstates in semiconductor gate-defined quantum-dot spin qubits. We use a system of four single-spin qubits, which we configure as two Ising-coupled singlet-triplet qubits. Our approach, which relies on the physics underlying discrete time crystals, enhances the quality factor of spin-eigenstate swaps by up to an order of magnitude. Our results show how interactions and disorder in multi-qubit systems can stabilize non-trivial quantum operations and suggest potential uses for non-equilibrium quantum phenomena, like time crystals, in quantum information processing applications.

INTRODUCTION

Over the past decades, quantum information processors have undergone remarkable progress, culminating in recent demonstrations of their astonishing power [1]. As quantum information processors continue to scale up in size and complexity, new challenges come to light. In particular, maintaining the performance of individual qubits and high connectivity are both essential for continued improvement in large systems [2].

At the same time, developments in non-equilibrium many-body physics have yielded insights into many-qubit phenomena, which feature, in some sense, improved performance of many-body quantum systems when disorder and interactions are included. Chief among these phenomena are many-body localization [3] and time crystals [4–8]. Although these phenomena are interesting in their own right, applications of these concepts are only beginning to emerge.

In this work, we incorporate the physics of time crystals in a multi-qubit processor to demonstrate Floquet-enhanced spin-eigenstate swaps in a system of four quantum-dot spin qubits. When we harness interactions and disorder in our system, the quality factor of spin-eigenstate swaps improves by nearly an order of magnitude. As we discuss in detail further below, this system of four exchange-coupled single-spin qubits undergoing repeated SWAP pulses maps onto a system of two Ising-coupled singlet-triplet qubits undergoing repeated π pulses. Periodically-driven Ising-coupled spin chains are the prototypical example of a system predicted to exhibit time-crystalline behavior [4]. Experimental signa-

tures of time-crystalline behavior have been observed in many systems [9–12], but nearest-neighbor Ising-coupled spin chains have yet to be experimentally investigated in this regard.

Our system of two singlet-triplet qubits is clearly not a time crystal in the strict sense, because it is not a many-body system [13]. However, this system does exhibit some of the key characteristics of time-crystalline behavior, including robustness against interactions, noise, and pulse imperfections [13, 14]. We also find that the required experimental conditions for observing the quality-factor enhancement are identical to some of the theoretical conditions for the time-crystal phase in infinite spin chains. In total, these observations suggest the Floquet-enhanced spin-eigenstate swaps in our device are closely related to discrete time-translation symmetry breaking.

Our results also illustrate how non-equilibrium many-body phenomena could potentially be used for quantum information processing. On the one hand, we observe Floquet-enhanced π rotations in two singlet-triplet qubits. But on the other hand, these singlet-triplet π rotations correspond to spin-eigenstate swaps when we view the system as four single spins. Given the critical importance of SWAP gates for information transfer in quantum systems [15, 16], these results may point the way toward the use of non-equilibrium quantum phenomena in quantum information processing applications, especially for initialization, readout, and information transfer.

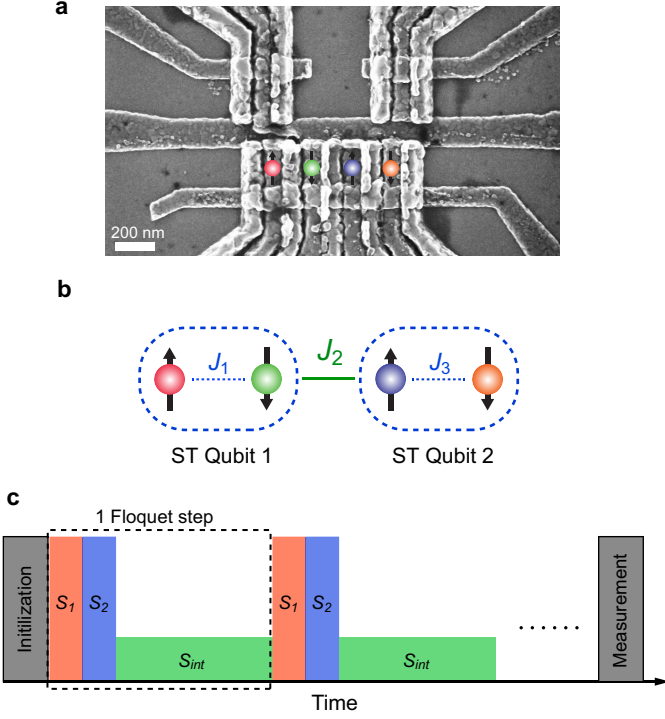


FIG. 1. Experimental setup. (a) Scanning electron micrograph of the quadruple quantum dot device. The locations of the electron spins are overlaid. (b) Schematic showing the two-qubit Ising system in a four-spin Heisenberg chain. (c) The pulse sequence used in the experiments.

DEVICE AND HAMILTONIAN

We fabricate a quadruple quantum dot array in a GaAs/AlGaAs heterostructure with overlapping gates [Fig. 1(a)] [17–19]. The confinement potentials of the dots are controlled through “virtual gates” [20–23]. Two extra quantum dots are placed nearby and serve as fast charge sensors [24, 25]. We configure the four-spin array into two pairs (“left” and “right”) for initialization and readout. Each pair of spins can be prepared in a product state ($|\uparrow\downarrow\rangle$ or $|\downarrow\uparrow\rangle$) via adiabatic separation of a singlet in the hyperfine gradient [15, 26, 27]. We can also initialize either pair as $|T_+\rangle = |\uparrow\uparrow\rangle$ by exchanging electrons with the reservoirs [27, 28]. Both pairs are measured through spin-to-charge conversion via Pauli spin blockade [26], together with a shelving mechanism [29] for high readout fidelity.

The four-spin array is governed by the following Hamiltonian:

$$H = \frac{\hbar}{4} \sum_{i=1}^3 J_i (\boldsymbol{\sigma}_i \cdot \boldsymbol{\sigma}_{i+1}) + \frac{\hbar}{2} \sum_{i=1}^4 B_i^z \sigma_i^z, \quad (1)$$

where J_i is the tunable exchange coupling strength (with units of frequency), $\boldsymbol{\sigma}_i = [\sigma_i^x, \sigma_i^y, \sigma_i^z]$ is the Pauli vector describing the components of spin i , \hbar is Planck’s

constant, and B_i^z is the z component of the magnetic field (also with units of frequency) experienced by spin i . B_i^z includes both a large 0.5-T external magnetic field and the smaller hyperfine field. The exchange couplings J_1 , J_2 , and J_3 are controlled by pulsing virtual barrier gate voltages [30]. We model the dependence of the exchange couplings on the virtual barrier gate voltages in the Heitler-London framework [30, 31]. The model allows us to predict the required barrier gate voltages for a set of desired exchange couplings. In our device, we estimate the residual exchange coupling at the idling tuning of the device to be a few MHz.

Heisenberg exchange coupling does not naturally enable the creation of a time-crystal phase [8]. Additional control pulses can convert the Heisenberg interaction into an Ising interaction [8], which permits the emergence of a time-crystal phase. A time crystal can also be created using a sufficiently strong magnetic field gradient instead of applying extra pulses [32]. Here, we introduce a new method for generating time-crystalline behavior that does not require complicated pulse sequences or large field gradients, but instead relies only on periodic exchange pulses. To see how we can still obtain an effective Ising interaction in this case, it helps to view each pair of spins as an individual singlet-triplet (ST) qubit [Fig. 1(b)] [26]. Specifically, consider the scenario where the joint spin-state of each pair is confined to the subspace spanned by $|S\rangle = \frac{1}{\sqrt{2}} (|\uparrow\downarrow\rangle - |\downarrow\uparrow\rangle)$ and $|T_0\rangle = \frac{1}{\sqrt{2}} (|\uparrow\uparrow\rangle + |\downarrow\downarrow\rangle)$. According to Ref. [33], when $J_1 = J_3 = 0$ and $J_2 > 0$, the effective Hamiltonian of the system is

$$H_{eff} = \frac{\hbar}{2} (\Delta_{12} + \bar{B}) \tilde{\sigma}_1^z + \frac{\hbar}{2} (\Delta_{34} + \bar{B}) \tilde{\sigma}_2^z - \frac{\hbar}{4} J_2 \tilde{\sigma}_1^z \tilde{\sigma}_2^z. \quad (2)$$

Here, $\tilde{\sigma}_k^z$ is the Pauli z -operator for ST qubit k , $\Delta_{ij} = B_i^z - B_j^z$ is the intraqubit gradient between spins i and j , and \bar{B} is the effective global magnetic field gradient, which depends on Δ_{ij} and J_i [33]. In this system, all magnetic gradients result from the hyperfine interaction between the electron and nuclear spins [34]. The gradients are quasistatic on typical qubit manipulation timescales [35]. The basis for the singlet-triplet qubit operator $\tilde{\sigma}^z$ is $\{|\uparrow\downarrow\rangle, |\downarrow\uparrow\rangle\}$ provided that $J_2 \ll |B_2 - B_3|$ [33, 35, 36]. In our experiments, the typical value of J_2 is a few MHz, while the typical value of the magnetic field gradient in the device is tens of MHz. Now let us define

$$S_{int} = \exp \left[-\frac{i}{\hbar} \tau \left(\frac{\hbar}{4} J_2 (\boldsymbol{\sigma}_2 \cdot \boldsymbol{\sigma}_3) + \frac{\hbar}{2} \sum_{i=1}^4 B_i^z \sigma_i^z \right) \right], \quad (3)$$

where τ is an interaction time. Within the $\{|S\rangle, |T_0\rangle\}$ subspace of each pair, this operator is equivalent to

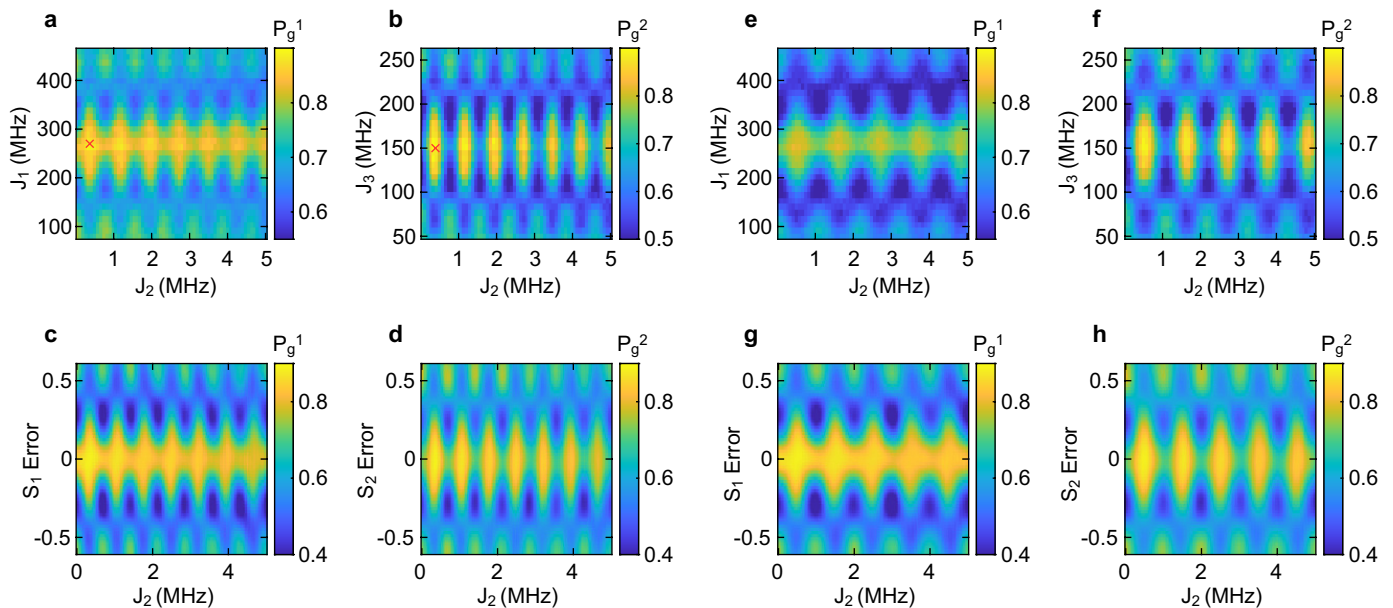


FIG. 2. Floquet-enhanced π rotations. (a-b) Measured ground state return probabilities of (a) ST qubit 1 and (b) ST qubit 2, after four Floquet steps, with interaction time $\tau = 1.4 \mu\text{s}$. The ranges of J_1 and J_3 center around the values such that S_1 and S_2 induce π pulses. The values of J_1 and J_3 are swept simultaneously. In both figures, the red cross marks the condition for the Floquet-enhanced π rotations. (c-d) Simulated return probabilities of (c) ST qubit 1 and (d) ST qubit 2, corresponding to the data in (a) and (b), respectively. “ S_1 Error” and “ S_2 Error” indicate the fractional error in the rotation angle of the π pulse applied to ST qubits 1 and 2, respectively. (e-f) Measured ground state return probabilities of (e) ST qubit 1 and (f) ST qubit 2, after four Floquet steps, with interaction time $\tau = 1.0 \mu\text{s}$. J_1 and J_3 values are the same as in (a) and (b). (g-h) Simulated return probabilities of (g) ST qubit 1 and (h) ST qubit 2, corresponding to the data in (e) and (f), respectively. The experimental data in (a,b,e,f) are averaged over 8192 realizations. In all figures, P_g^k indicates the ground state return probability for ST qubit k .

$S_{int}^{eff} = \exp[-\frac{i}{\hbar}\tau H_{eff}]$, and it describes the evolution of the two Ising-coupled qubits [33]. Systems of exchange-coupled singlet-triplet qubits have been the focus of intense theoretical research [33, 37–39]. Until now, such a system has evaded implementation.

In the case when $J_2 = 0$, but when $J_1, J_3 > 0$, the overall Hamiltonian describes two uncoupled singlet-triplet qubits. Thus, let us define

$$S_1 = \exp\left[-\frac{i}{\hbar}t_1\left(\frac{\hbar}{4}J_1(\boldsymbol{\sigma}_1 \cdot \boldsymbol{\sigma}_2) + \frac{\hbar}{2}\sum_{i=1}^4 B_i^z \sigma_i^z\right)\right], \quad (4)$$

$$S_2 = \exp\left[-\frac{i}{\hbar}t_2\left(\frac{\hbar}{4}J_3(\boldsymbol{\sigma}_3 \cdot \boldsymbol{\sigma}_4) + \frac{\hbar}{2}\sum_{i=1}^4 B_i^z \sigma_i^z\right)\right]. \quad (5)$$

In the $\{|S\rangle, |T_0\rangle\}$ subspace of each pair, these operators are equivalent to $S_1^{eff} = \exp[-\frac{i}{\hbar}t_1\frac{\hbar}{2}(\Delta_{12}\tilde{\sigma}_1^z + J_1\tilde{\sigma}_1^x)]$ and $S_2^{eff} = \exp[-\frac{i}{\hbar}t_2\frac{\hbar}{2}(\Delta_{34}\tilde{\sigma}_2^z + J_3\tilde{\sigma}_2^x)]$. In writing S_1^{eff} and S_2^{eff} , we have ignored overall energy shifts $J_1/4$ and $J_3/4$ of the single-qubit Hamiltonians, because the system dynamics do not depend on these shifts. Assuming $J_1 \gg \Delta_{12}$ and $J_3 \gg \Delta_{34}$, when $t_1 J_1 = t_2 J_3 = 0.5$, these two operators implement SWAP gates between spins 1-2 and 3-4. Equivalently, they induce nominal π pulses about the x axis of each singlet-triplet qubit.

The presence of the intraqubit gradients Δ_{12} and Δ_{34} slightly tilts the rotation axis towards the z axis for each singlet-triplet qubit, introducing uncontrolled errors to the π pulses. We can also manually introduce additional pulse errors by changing J_1 and J_3 while fixing t_1 and t_2 .

FLOQUET-ENHANCED SPIN SWAPS

We define a Floquet operator $U = S_{int} \cdot S_2 \cdot S_1$ [Fig. 1(c)], and we repeatedly apply this operator to our system of four spins. As discussed above, U implements spin SWAP gates between spins 1-2 and 3-4 followed by a period of exchange interaction between spins 2 and 3. Equivalently, U implements π pulses on both ST qubits and then a period of Ising coupling between them. One might naively imagine that the highest fidelity SWAP operations between spins should occur when $J_2 = 0$ and $\tau = 0$, given the presence of intraqubit hyperfine gradients. In this case, as we have discussed in Ref. [15], repeated SWAP operations are especially susceptible to errors from the hyperfine gradients Δ_{ij} .

However, by allowing $J_2 > 0$ and $\tau > 0$, we find specific conditions in which we observe a significant enhancement of the spin-swap quality factor [Fig. 2]. To explore this

phenomenon, we prepare each ST qubit in $|\uparrow\downarrow\rangle$ or $|\downarrow\uparrow\rangle$. (The specific state is governed by the sign of Δ_{12} and Δ_{34} , which are random quasistatic gradients resulting from the nuclear hyperfine interaction.) We apply multiple instances of the Floquet operator U to the system and measure the ground state return probabilities for both ST qubits.

First we set the interaction time $\tau = 1.4 \mu\text{s}$ and SWAP pulse times $t_1 = t_2 = 5 \text{ ns}$, and apply four Floquet steps. We sweep J_2 linearly from 0.05 MHz to 5 MHz. (Setting $J_2 < 0.05 \text{ MHz}$ would require large negative voltage pulses applied to the barrier gate due to the residual exchange, which could disrupt the tuning of the device.) We also sweep J_1 from 80 MHz to 460 MHz, and J_3 from 50 MHz to 260 MHz. The ranges of J_1 and J_3 roughly center around the values at which S_1 and S_2 induce π pulses. Away from the center, J_1 and J_3 induce pulse errors. The experimental values of $t_1 J_1$ and $t_2 J_3$ for π pulses are much larger than 0.5, because the voltage pulses experienced by the qubits have rise times of about 1 ns. To compensate for the pulse rise times (which are slightly different for each qubit), $t_1 J_1$ and $t_2 J_3$ must be larger than 0.5 in order to properly induce π pulses.

Clear, bright diamond patterns are visible in the data [Fig. 2(a-b)]. These bright regions correspond to improved spin-eigenstate-swap quality factors. Note that the brightest regions correspond to configurations when $J_2 > 0$. Note also that the diamonds are approximately periodic in $J_2\tau$, as expected for a Floquet operator. We repeat the same experiments with $\tau = 1 \mu\text{s}$, and we observe similar diamond patterns, although they have an increased period in J_2 [Fig. 2(e-f)]. The diamond patterns of ST qubit 2 appear narrower due to the large hyperfine gradient Δ_{34} , which causes larger pulse errors and reduces the size of the quality-factor-enhancement region. These data from the two-qubit system resemble predicted time-crystal phase diagrams of a true many-body system [7, 8].

Our simulations agree well with the data [Fig. 2(c-d), (e-h)] (see Supplementary Material). In the simulations, the diamond pattern is periodic in $J_2\tau$ with the periodicity of exactly 1, and the strongest quality-factor enhancement occurs at $J_2\tau = 0.5$. In the experimental data, however, the periodicity is slightly larger than 1, and the strongest quality-factor enhancement occurs at $J_2\tau \approx 0.57$. This is due to the imperfect calibration of the exchange coupling J_2 [30]. In particular, the presence of the hyperfine field gradient makes it difficult to measure and control the exchange couplings with sub-MHz resolution. If our modeling of the exchange coupling were more precise, then we would expect the periodicity of the diamond patterns to be closer to 1 and the quality-factor enhancement to occur closer to $J_2\tau = 0.5$ in the experimental data.

Next, we sweep J_3 from 220 MHz to 430 MHz. In this case, the range of J_3 roughly centers around the

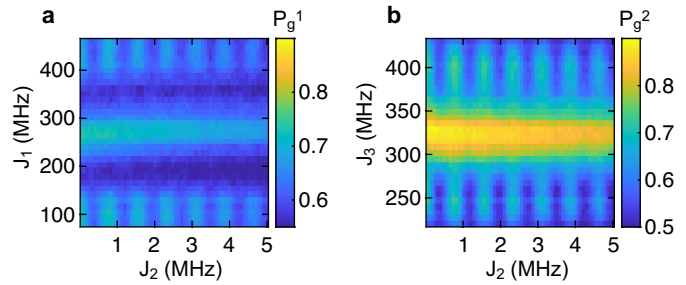


FIG. 3. Absence of Floquet enhancement due to the omission of a π pulse. (a-b) Measured ground state return probabilities of (a) ST qubit 1 and (b) ST qubit 2, after four Floquet steps, with interaction time $\tau = 1.4 \mu\text{s}$. The range of J_1 centers around the value such that S_1 induces a π pulse, while the range of J_3 centers around the value such that S_2 induces a 2π pulse. The values of J_1 and J_3 are swept simultaneously. The data are averaged over 8192 realizations.

value where S_2 induces a 2π rotation. The interaction time is $\tau = 1.4 \mu\text{s}$ and the ranges of J_1 and J_2 remain the same. Again we apply four Floquet steps and measure the ground state return probabilities. This time the data do not show diamond patterns [Fig. 3], and the return probability of ST qubit 1 is lower than the Floquet-enhanced return probability shown in Fig. 2(a). This indicates that the Floquet enhancement is no longer present. In fact, if either of the Floquet operators S_1 or S_2 fails to induce approximately a π rotation, then the Floquet enhancement does not appear.

We emphasize the striking nature of this effect. Recall that the ST qubit splittings Δ_{12} and Δ_{34} are generated by the hyperfine interaction between the Ga and As nuclei in the semiconductor heterostructure and the electron spins in the quantum dots. Although Δ_{12} and Δ_{34} are quasistatic on millisecond timescales, they each independently fluctuate randomly over the duration of a typical data-taking run, which is about one hour. Thus at any given time, the state of each ST qubit before any Floquet operators are applied is either $|\uparrow\downarrow\rangle$ or $|\downarrow\uparrow\rangle$. The data of Fig. 2 include realizations with all possible combinations of the orientations of spins 2 and 3 before the interaction period. Despite the random orientations of spins 2 and 3, the Floquet enhancement still appears. It might therefore seem that whether or not spins 1-2 or 3-4 undergo a SWAP before the interaction period should not affect the behavior of the system. However, as shown in Fig. 3, implementing a 2π rotation, as opposed to a π rotation, on one of the ST qubits eliminates the Floquet enhancement. As we discuss below, the lack of *global* π pulses violates a requirement for discrete time-translation symmetry breaking.

We have now determined the optimal conditions for the Floquet enhancement. For the remainder of the paper, we set $J_1 = 270 \text{ MHz}$ and $J_3 = 150 \text{ MHz}$ with $t_1 = t_2 = 5 \text{ ns}$ for the SWAP operators S_1 and S_2 , respec-

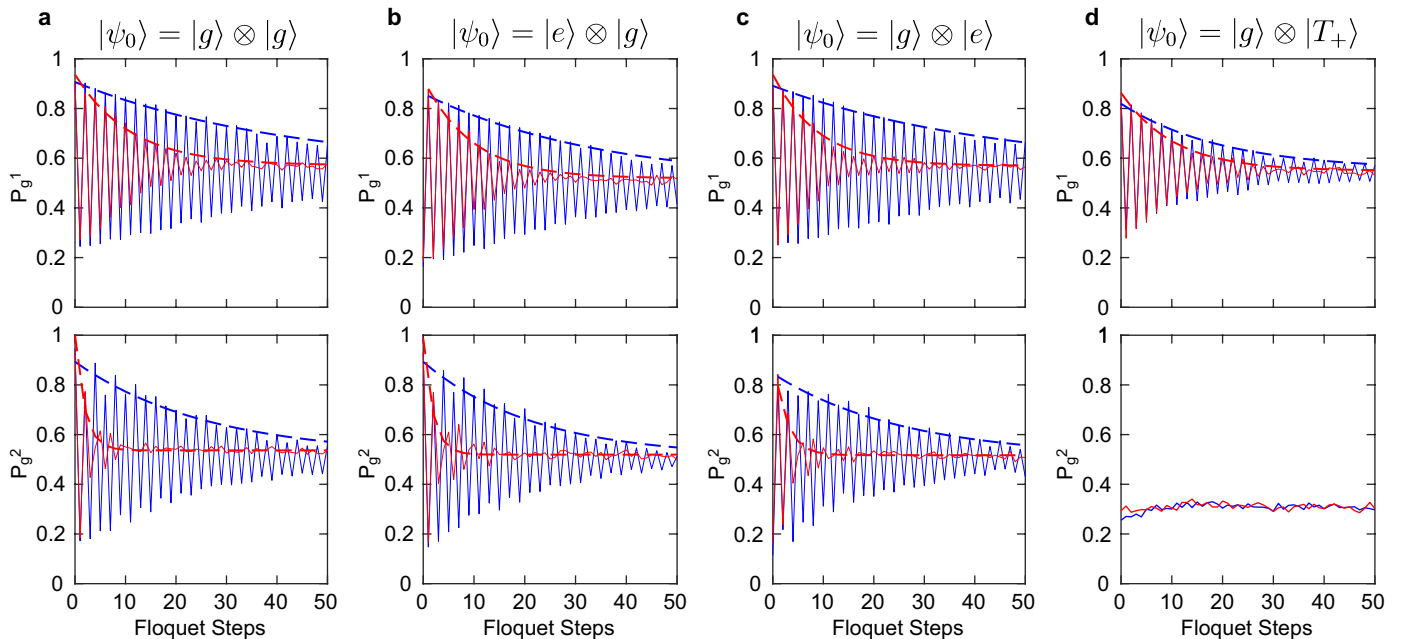


FIG. 4. (a-d) Quality-factor enhancement of spin-eigenstate swaps for different initial states. In each figure, the top panel shows the measurements of ST qubit 1, and the bottom panel shows the measurements of ST qubit 2. The initial states are shown on the top, where $|g\rangle$ and $|e\rangle$ represent the ground state and the excited state of the ST qubit, respectively. The Floquet-enhanced π -pulse data are shown in blue, and the non-enhanced regular π -pulse data are shown in red. The fitted exponential decay envelopes are overlaid as dashed lines for all data except for the bottom panel in (d). The data are averaged over 4096 realizations

tively, and we set $\tau = 1.4 \mu\text{s}$ and $J_2 = 0.41 \text{ MHz}$ for the Ising interaction. To quantify the Floquet enhancement, we evolve the system for 50 Floquet steps and measure the ground state return probabilities for both qubits after each step. The results are shown in Fig. 4(a). Note that the system exhibits a clear subharmonic response to the Floquet operator. We extract a swap quality Q by fitting the data with a decaying sinusoidal function $P_g(n) = \alpha \exp(-n/Q) \cos(n\pi) + \beta$, where $P_g(n)$ denotes the return probability at the n th Floquet step, and Q , α , and β are fit parameters. We also investigate the quality factor of the qubits under non-enhanced regular π pulses. Here we use the same interaction time $\tau = 1.4 \mu\text{s}$, but we turn off the interaction strength J_2 by setting the barrier-gate pulse to zero. To further eliminate any effects associated with Floquet enhancement, we only apply π pulses to one qubit while the other qubit remains idle after initialization. Again, we apply 50 π pulses and measure the ground state return probability, and we fit the data with the same decaying sinusoidal function. By comparing the fit parameter Q , we can obtain the ratio between the quality factors of the qubits under Floquet-enhanced and non-enhanced π rotations.

We find a ~ 3 -fold quality-factor improvement on qubit 1, and ~ 9 -fold improvement on qubit 2. The significant discrepancy between the quality-factor improvements of the two qubits is likely due to the large hyperfine gradient Δ_{34} in qubit 2, which causes an exceptionally low quality

factor for non-enhanced π rotations. The quality-factor enhancement is striking in this case. To extract an estimated uncertainty, we repeat the same experiment 30 times and calculate the mean and the variance of the quality factor ratio, as shown in the first row of Table I.

So far, we have initialized both ST qubits in their ground states. We can also initialize either ST qubit in its excited state by applying an extra π pulse to the qubit immediately before the first Floquet step. We run the same experiment with different initial states and extract the quality factors by fitting the data [Fig. 4(b-c)]. Again, for each initial state, we repeat the experiment 30 times and calculate the mean and the variance of the

Initialization	Quality-factor enhancement	
	Qubit 1	Qubit 2
$ g\rangle \otimes g\rangle$	3.60 ± 0.89	8.47 ± 3.29
$ e\rangle \otimes g\rangle$	3.24 ± 0.94	9.33 ± 2.96
$ g\rangle \otimes e\rangle$	3.15 ± 0.79	9.10 ± 2.87
$ g\rangle \otimes T_+\rangle$	1.92 ± 0.27	N/A

TABLE I. Quality-factor enhancements of both qubits for different initial states. Here $|g\rangle$ and $|e\rangle$ represent the ground state and the excited state of the ST qubit, respectively. Thirty sets of data are taken for each initialization, from which the means and the standard deviations are calculated.

quality-factor ratio, which are listed in Table I. The quality-factor improvements of both qubits are consistent across different initial states. We also initialize qubit 2 as $|T_+\rangle = |\uparrow\uparrow\rangle$ and measure the quality-factor improvement on qubit 1 [Fig. 4(d)]. We notice that the quality-factor ratio is much lower when qubit 2 is initialized in $|T_+\rangle$. This is not surprising since the effective Ising interaction between qubit 1 and qubit 2 (Eq. 2) is only valid when both qubits are restricted to the $s_z = 0$ subspace. The reason why we still see a ~ 2 -fold quality-factor improvement instead of no improvement at all is likely because of the imperfect $|T_+\rangle$ preparation due to thermal population of excited states [28]. ST qubit 2 has non-zero probability after the $|T_+\rangle$ initialization to remain in the $s_z = 0$ subspace, which enables weak Floquet enhancement.

DISCUSSION

Strictly speaking, a discrete time crystal only occurs in the many-body limit [13]. Nonetheless, we argue the quality-factor enhancement we observe relies on the essential elements of time-crystal physics. The disordered Ising-coupled system in our device demonstrates a clear subharmonic response as well as a robustness against pulse errors, both expected as defining signatures of the discrete time crystal. Our experiments also indicate the necessity of two essential ingredients for realizing the Floquet-enhanced π pulses: 1) an effective Ising interaction, and 2) *global* π pulses. If either of the components is missing, we no longer observe the significant quality-factor enhancement [Figs. 3 and 4(d)]. These two components both ensure that the eigenstates of the Floquet operator are long-range correlated and are required for discrete time-translation symmetry breaking [5]. In particular, replacing a π pulse with a 2π pulse on any of the spins in the Ising spin chain causes the Floquet eigenstates to be short-range correlated (see Supplementary Material). Furthermore, we have also shown that the quality-factor enhancement does not depend on the choice of initial state of the qubits (provided that the effective Ising model is maintained), which is another key feature of the discrete time crystal [13]. In the future, implementing these experiments in larger spin chains could lead to a verification that these effects in fact originate from the time crystal phase.

We emphasize that we have observed Floquet enhancement associated with ST-qubit eigenstates undergoing π pulses. In the language of single spins, we observed Floquet enhancement associated with swaps between spin eigenstates, when the total z component of angular momentum for both spins vanishes. This observation is qualitatively consistent with expectations for qubits in a true many-body time crystal, where the components of the qubits oriented along the direction defined by the

Ising coupling are preserved [8]. While not a coherent SWAP gate, a spin-eigenstate swap has significant potential to aid in readout for large qubit arrays [16]. The potential application of Floquet techniques to superposition states of singlet-triplet qubits remains an important subject of future work. Finally, we expect that Floquet-enhanced spin swaps can also be achieved in Si spin qubits. Barrier-controlled exchange coupling between Si spin qubits is now routine [40]. The operation of Si singlet-triplet qubits in the regime where magnetic gradients exceed exchange couplings has also been demonstrated [41, 42].

CONCLUSION

In summary, we have demonstrated Floquet-enhanced spin-eigenstate swaps in a four-spin two-qubit Ising chain in a quadruple quantum-dot array. The system shows a subharmonic response to the driving frequency, and it also shows an improvement in swap quality factor even in the presence of pulse imperfections. We have also shown that the necessary conditions for this quality-factor enhancement are identical to some key components for realizing discrete time crystals. Our results indicate the possibility of realizing discrete time crystals using extended Heisenberg spin chains in semiconductor quantum dots, and suggest potential uses for quantum information processing applications.

ACKNOWLEDGMENTS

This research was sponsored by the Defense Advanced Research Projects Agency under Grant No. D18AC00025, the Army Research Office under Grant Nos. W911NF16-1-0260 and W911NF-19-1-0167, and the National Science Foundation under Grant No. DMR-1941673. The views and conclusions contained in this document are those of the authors and should not be interpreted as representing the official policies, either expressed or implied, of the Army Research Office or the U.S. Government. The U.S. Government is authorized to reproduce and distribute reprints for Government purposes notwithstanding any copyright notation herein.

* john.nichol@rochester.edu

[1] F. Arute, K. Arya, R. Babbush, D. Bacon, J. C. Bardin, R. Barends, R. Biswas, S. Boixo, F. G. S. L. Brandao, D. A. Buell, B. Burkett, Y. Chen, Z. Chen, B. Chiaro, R. Collins, W. Courtney, A. Dunsworth, E. Farhi, B. Foxen, A. Fowler, C. Gidney, M. Giustina, R. Graff, K. Guerin, S. Habegger, M. P. Harrigan, M. J. Hartmann, A. Ho, M. Hoffmann, T. Huang,

- T. S. Humble, S. V. Isakov, E. Jeffrey, Z. Jiang, D. Kafri, K. Kechedzhi, J. Kelly, P. V. Klimov, S. Knysh, A. Korotkov, F. Kostritsa, D. Landhuis, M. Lindmark, E. Lucero, D. Lyakh, S. Mandrà, J. R. McClean, M. McEwen, A. Megrant, X. Mi, K. Michielsen, M. Mohseni, J. Mutus, O. Naaman, M. Neeley, C. Neill, M. Y. Niu, E. Ostby, A. Petukhov, J. C. Platt, C. Quintana, E. G. Rieffel, P. Roushan, N. C. Rubin, D. Sank, K. J. Satzinger, V. Smelyanskiy, K. J. Sung, M. D. Trethick, A. Vainsencher, B. Villalonga, T. White, Z. J. Yao, P. Yeh, A. Zalcman, H. Neven, and J. M. Martinis, *Nature* **574**, 505 (2019).
- [2] N. M. Linke, D. Maslov, M. Roetteler, S. Debnath, C. Figgatt, K. A. Landsman, K. Wright, and C. Monroe, *Proceedings of the National Academy of Sciences* **114**, 3305 (2017).
- [3] A. Pal and D. A. Huse, *Phys. Rev. B* **82**, 174411 (2010).
- [4] V. Khemani, A. Lazarides, R. Moessner, and S. L. Sondhi, *Phys. Rev. Lett.* **116**, 250401 (2016).
- [5] D. V. Else, B. Bauer, and C. Nayak, *Phys. Rev. Lett.* **117**, 090402 (2016).
- [6] C. W. von Keyserlingk and S. L. Sondhi, *Phys. Rev. B* **93**, 245146 (2016).
- [7] N. Y. Yao, A. C. Potter, I.-D. Potirniche, and A. Vishwanath, *Phys. Rev. Lett.* **118**, 030401 (2017).
- [8] E. Barnes, J. M. Nichol, and S. E. Economou, *Phys. Rev. B* **99**, 035311 (2019).
- [9] J. Zhang, P. W. Hess, A. Kyprianidis, P. Becker, A. Lee, J. Smith, G. Pagano, I.-D. Potirniche, A. C. Potter, A. Vishwanath, N. Y. Yao, and C. Monroe, *Nature* **543**, 217 (2017).
- [10] S. Choi, J. Choi, R. Landig, G. Kucsko, H. Zhou, J. Isoya, F. Jelezko, S. Onoda, H. Sumiya, V. Khemani, C. von Keyserlingk, N. Y. Yao, E. Demler, and M. D. Lukin, *Nature* **543**, 221 (2017).
- [11] J. Rovny, R. L. Blum, and S. E. Barrett, *Phys. Rev. Lett.* **120**, 180603 (2018).
- [12] S. Pal, N. Nishad, T. S. Mahesh, and G. J. Sreejith, *Phys. Rev. Lett.* **120**, 180602 (2018).
- [13] V. Khemani, R. Moessner, and S. L. Sondhi, “A brief history of time crystals,” (2019), arXiv:1910.10745 [cond-mat.str-el].
- [14] C. W. von Keyserlingk, V. Khemani, and S. L. Sondhi, *Phys. Rev. B* **94**, 085112 (2016).
- [15] Y. P. Kandel, H. Qiao, S. Fallahi, G. C. Gardner, M. J. Manfra, and J. M. Nichol, *Nature* **573**, 553 (2019).
- [16] A. Sigillito, J. Loy, D. Zajac, M. Gullans, L. Edge, and J. Petta, *Phys. Rev. Applied* **11**, 061006 (2019).
- [17] S. J. Angus, A. J. Ferguson, A. S. Dzurak, and R. G. Clark, *Nano Letters* **7**, 2051 (2007).
- [18] D. M. Zajac, T. M. Hazard, X. Mi, K. Wang, and J. R. Petta, *Applied Physics Letters* **106**, 223507 (2015).
- [19] D. M. Zajac, T. M. Hazard, X. Mi, E. Nielsen, and J. R. Petta, *Phys. Rev. Applied* **6**, 054013 (2016).
- [20] T. A. Baart, M. Shafiei, T. Fujita, C. Reichl, W. Wegscheider, and L. M. K. Vandersypen, *Nature Nanotechnology* **11**, 330 EP (2016).
- [21] T. Hensgens, T. Fujita, L. Janssen, X. Li, C. J. Van Diepen, C. Reichl, W. Wegscheider, S. Das Sarma, and L. M. K. Vandersypen, *Nature* **548**, 70 EP (2017).
- [22] C. Volk, A. M. J. Zwerver, U. Mukhopadhyay, P. T. Eendebak, C. J. van Diepen, J. P. Dehollain, T. Hensgens, T. Fujita, C. Reichl, W. Wegscheider, and L. M. K. Vandersypen, *npj Quantum Information* **5**, 29 (2019).
- [23] A. R. Mills, M. M. Feldman, C. Monical, P. J. Lewis, K. W. Larson, A. M. Mounce, and J. R. Petta, *Applied Physics Letters* **115**, 113501 (2019).
- [24] D. J. Reilly, C. M. Marcus, M. P. Hanson, and A. C. Gossard, *Applied Physics Letters* **91**, 162101 (2007).
- [25] C. Barthel, M. Kjærgaard, J. Medford, M. Stopa, C. M. Marcus, M. P. Hanson, and A. C. Gossard, *Phys. Rev. B* **81**, 161308 (2010).
- [26] J. R. Petta, A. C. Johnson, J. M. Taylor, E. A. Laird, A. Yacoby, M. D. Lukin, C. M. Marcus, M. P. Hanson, and A. C. Gossard, *Science* **309**, 2180 (2005).
- [27] S. Foletti, H. Bluhm, D. Mahalu, V. Umansky, and A. Yacoby, *Nature Physics* **5**, 903 (2009).
- [28] L. A. Orona, J. M. Nichol, S. P. Harvey, C. G. L. Böttcher, S. Fallahi, G. C. Gardner, M. J. Manfra, and A. Yacoby, *Phys. Rev. B* **98**, 125404 (2018).
- [29] S. A. Studenikin, J. Thorgrimson, G. C. Aers, A. Kam, P. Zawadzki, Z. R. Wasilewski, A. Bogan, and A. S. Sachrajda, *Applied Physics Letters* **101**, 233101 (2012).
- [30] H. Qiao, Y. P. Kandel, K. Deng, S. Fallahi, G. C. Gardner, M. J. Manfra, E. Barnes, and J. M. Nichol, “Coherent multi-spin exchange in a quantum-dot spin chain,” (2020), arXiv:2001.02277 [cond-mat.mes-hall].
- [31] R. de Sousa, X. Hu, and S. Das Sarma, *Phys. Rev. A* **64**, 042307 (2001).
- [32] B. Li, J. S. Van Dyke, A. Warren, S. E. Economou, and E. Barnes, *Phys. Rev. B* **101**, 115303 (2020).
- [33] M. P. Wardrop and A. C. Doherty, *Phys. Rev. B* **90**, 045418 (2014).
- [34] J. M. Taylor, J. R. Petta, A. C. Johnson, A. Yacoby, C. M. Marcus, and M. D. Lukin, *Phys. Rev. B* **76**, 035315 (2007).
- [35] M. D. Shulman, S. P. Harvey, J. M. Nichol, S. D. Bartlett, A. C. Doherty, V. Umansky, and A. Yacoby, *Nature Communications* **5**, 5156 (2014).
- [36] J. M. Nichol, L. A. Orona, S. P. Harvey, S. Fallahi, G. C. Gardner, M. J. Manfra, and A. Yacoby, *npj Quantum Information* **3**, 3 (2017).
- [37] J. Levy, *Phys. Rev. Lett.* **89**, 147902 (2002).
- [38] J. Klinovaja, D. Stepanenko, B. I. Halperin, and D. Loss, *Phys. Rev. B* **86**, 085423 (2012).
- [39] R. Li, X. Hu, and J. Q. You, *Phys. Rev. B* **86**, 205306 (2012).
- [40] M. D. Reed, B. M. Maune, R. W. Andrews, M. G. Borselli, K. Eng, M. P. Jura, A. A. Kiselev, T. D. Ladd, S. T. Merkel, I. Milosavljevic, E. J. Pritchett, M. T. Rakher, R. S. Ross, A. E. Schmitz, A. Smith, J. A. Wright, M. F. Gyure, and A. T. Hunter, *Phys. Rev. Lett.* **116**, 110402 (2016).
- [41] A. J. Sigillito, M. J. Gullans, L. F. Edge, M. Borselli, and J. R. Petta, *npj Quantum Information* **5**, 110 (2019).
- [42] K. Takeda, A. Noiri, J. Yoneda, T. Nakajima, and S. Tarucha, *Phys. Rev. Lett.* **124**, 117701 (2020).

Supplementary Material for Floquet-Enhanced Spin Swaps

Haifeng Qiao,¹ Yadav P. Kandel,¹ John S. Van Dyke,² Saeed Fallahi,^{3,4} Geoffrey C. Gardner,^{4,5} Michael J. Manfra,^{3,4,5,6} Edwin Barnes,² and John M. Nichol^{1,*}

¹*Department of Physics and Astronomy,
University of Rochester, Rochester, NY, 14627 USA*

²*Department of Physics, Virginia Tech, Blacksburg, Virginia, 24061, USA*

³*Department of Physics and Astronomy,
Purdue University, West Lafayette, IN, 47907 USA*

⁴*Birck Nanotechnology Center, Purdue University, West Lafayette, IN, 47907 USA*

⁵*School of Materials Engineering, Purdue University, West Lafayette, IN, 47907 USA*

⁶*School of Electrical and Computer Engineering,
Purdue University, West Lafayette, IN, 47907 USA*

A. Device

The quadruple quantum dot device is fabricated on a GaAs/AlGaAs heterostructure substrate with three layers of overlapping Al confinement gates and a final Al top gate. The Al gates are patterned and deposited using E-beam lithography and thermal evaporation, and each layer is isolated from the other layers by a few nanometers of native oxide. The top gate covers the main device area and is grounded during the experiments. It likely smooths anomalies in the quantum dot potentials. The two-dimensional electron gas resides at the GaAs and AlGaAs interface, 91 nm below the semiconductor surface. The device is cooled in a dilution refrigerator with base temperature of approximately 10 mK. A 0.5-T external magnetic field is applied parallel to the device surface and perpendicular to the axis connecting the quantum dots.

* john.nichol@rochester.edu

B. Simulation

We simulate the Floquet-enhanced phenomena by evolving a four-spin array according to the Floquet operator $U = S_{int} \cdot S_2 \cdot S_1$, as defined in the main text. We set $t_1 = t_2 = 2$ ns, and $J_1 = J_3 = 250$ MHz for the SWAP operators S_1 and S_2 to give π pulses. While t_1 and t_2 are chosen to be 5 ns in the experiments, we expect the realistic SWAP times to be approximately 2~3 ns due to the pulse rise and fall times of about 1 ns. We include the π -pulse errors by adjusting the exchange couplings as $J_1(1 + \epsilon_1)$ and $J_3(1 + \epsilon_2)$, where ϵ_1 and ϵ_2 represent the fractional error in the rotation angle of the π pulse applied to ST qubit 1 and 2, respectively.

For better comparison with the experimental data, the simulations take into account all known error sources, including state preparation, readout, charge noise, and hyperfine field noise. The initial state of each ST qubit is prepared as

$$|\psi_i\rangle = s_1 |g\rangle + s_2 |e\rangle + s_3 |T_+\rangle + s_4 |T_-\rangle, \quad (1)$$

where $|g\rangle$ and $|e\rangle$ are the ground state and the excited state in the $\{|\uparrow\downarrow\rangle, |\downarrow\uparrow\rangle\}$ basis. The exact spin orientation for the ground state is determined by the hyperfine gradient. The coefficient $|s_1|^2 = f_g$ represents the ground state preparation fidelity, and we assume $|s_2|^2 = |s_3|^2 = |s_4|^2 = \frac{1}{3}(1 - f_g)$ for simplicity. We estimate f_g to be 0.9 for ST qubit 1 and 0.95 for ST qubit 2 in our device. The preparation fidelity assumes errors from both the singlet loading and the charge separation. The readout errors are included by calculating the final ground state return probability as

$$\tilde{P}_g = (1 - r - 2q)P_g + r + q, \quad (2)$$

where $P_g = |\langle g|\psi_f\rangle|^2$ is the true ground state return probability. Here $r = 1 - \exp(-t_m/T_1)$ is the probability of the excited state relaxing to the ground state during measurements, with t_m being the measurement time and T_1 being the relaxation time. Also $q = 1 - f_m$ is the probability of misidentifying the ground state as the excited state due to random noise. We set $t_m = 4 \mu\text{s}$, $T_1 = 60 \mu\text{s}$, and $f_m = 0.99$ for ST qubit 1, and $t_m = 6 \mu\text{s}$, $T_1 = 50 \mu\text{s}$, and $f_m = 0.95$ for ST qubit 2.

We use a Monte-Carlo method to incorporate charge noise and hyperfine field fluctuations. The values of the exchange couplings J_i and the local hyperfine fields B_i^z are randomly

sampled from a normal distribution for each simulation run. We set the standard deviation for J_i to be $J_i/(\sqrt{2}\pi Q)$, where $Q = 21$ is the exchange oscillation quality factor. We set the standard deviation for B_i^z to be 18 MHz, and we assume the mean values to be $[0, 20, 0, 50]$ MHz plus a uniform magnetic field of 3.075 GHz (which accounts for the 0.5-T external magnetic field). The simulated data in Fig. 2 in the main text are obtained by averaging over 128 realizations.

C. Discrete Time-Translation Symmetry Breaking

A key definition of discrete time-translation symmetry breaking is that all eigenstates of the Floquet operator are exclusively long-range correlated [1]. The definition is violated if a π pulse in the Floquet operator is omitted (or, equivalently, replaced by a 2π pulse), which we explicitly show here.

Consider an infinite Ising spin chain, with Hamiltonian

$$H = \frac{\hbar}{4} \sum_i J \sigma_i^z \sigma_{i+1}^z + \frac{\hbar}{2} \sum_i B_i^z \sigma_i^z. \quad (3)$$

The eigenstates of this Hamiltonian are those states with definite spin at each site. Following Ref. [1], denote such a state as

$$|\phi_1\rangle = |s_1, s_2, \dots, s_{j-1}, s_j, s_{j+1}, \dots\rangle, \quad (4)$$

where $s_i = \pm 1$ and $\sigma_i^z |\phi_1\rangle = s_i |\phi_1\rangle$. Then, $H |\phi_1\rangle = E_1 |\phi_1\rangle$. Let us consider another eigenstate

$$|\phi_2\rangle = |-s_1, -s_2, \dots, -s_{j-1}, s_j, -s_{j+1}, \dots\rangle, \quad (5)$$

with $H |\phi_2\rangle = E_2 |\phi_2\rangle$. Relative to $|\phi_1\rangle$, all of the spins, except for the j th spin, have been flipped in $|\phi_2\rangle$.

Denote a Floquet operator

$$U(t) = \exp\left(-\frac{i}{\hbar} H t\right) \cdot \prod_{i \neq j} \sigma_i^x. \quad (6)$$

where σ_i^x indicates a π rotation about the x -axis for spin i . Note that the π rotation for spin j is omitted here. Set $\Delta = E_2 - E_1$ and $\Sigma = E_2 + E_1$. It is easily verified by explicit computation that the state

$$|\psi\rangle = \frac{1}{\sqrt{2}} \left[\exp\left(\frac{i\Delta t}{4\hbar}\right) |\phi_1\rangle \pm \exp\left(-\frac{i\Delta t}{4\hbar}\right) |\phi_2\rangle \right] \quad (7)$$

is an eigenstate of $U(t)$ with eigenvalue $\pm \exp(-i\Sigma t/2\hbar)$. We can determine whether the state $|\psi\rangle$ is long-range correlated by noticing that

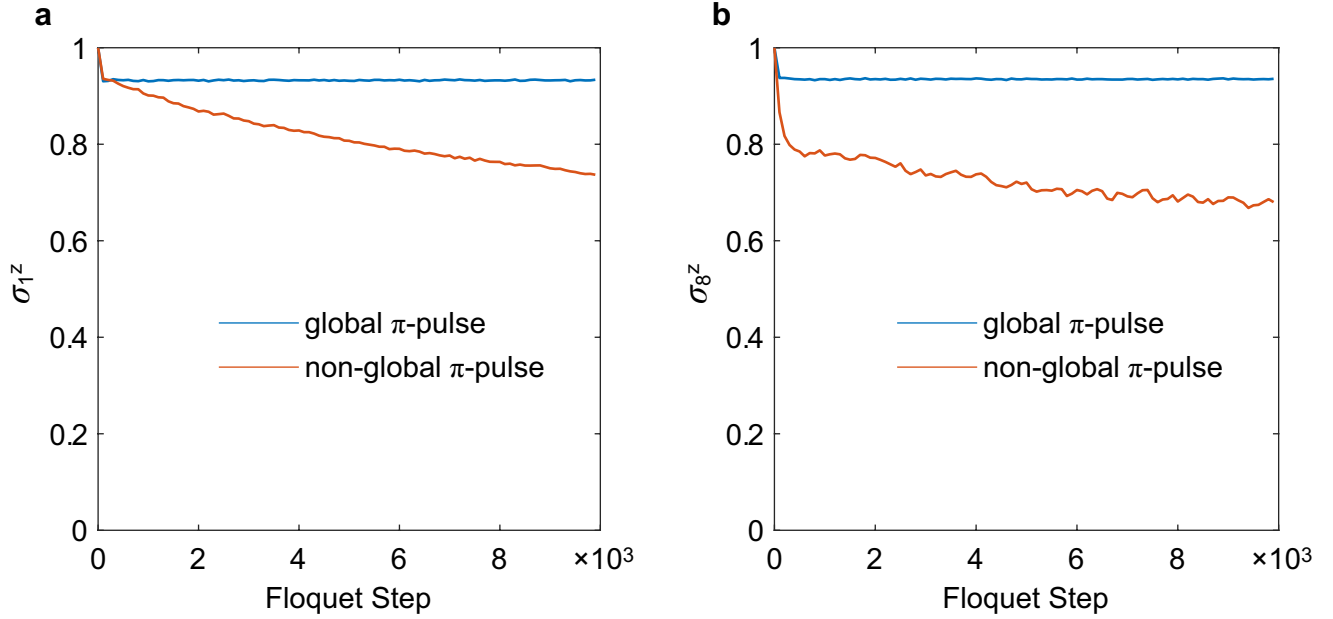
$$R_k^z \equiv \lim_{|k-j| \rightarrow \infty} [\langle \psi | \sigma_j^z \sigma_k^z | \psi \rangle - \langle \psi | \sigma_j^z | \psi \rangle \langle \psi | \sigma_k^z | \psi \rangle] = 0. \quad (8)$$

According to Refs. [1, 2], this value of R_k^z implies that $|\psi\rangle$ is short-range correlated, and the time crystal phase is not allowed in this system.

To further examine the effect of omitting a π pulse, we simulate the time evolution of an $N = 8$ Ising spin chain under the Floquet operator. Supplementary Fig. 1 shows the expectation values of the Pauli z -operator for the two end spins over 10000 Floquet steps. The simulated data are averaged over 512 disorder realizations. We notice that, by replacing the π pulse for spin 5 with a 2π pulse, the long-time stability of the end spin is significantly affected, which indicates the time crystal phase is destroyed by the absence of a π pulse.

By showing that applying global π pulses is indeed an essential component of creating a discrete time crystal, we have further confirmed the observed Floquet-enhanced spin swap in our system is associated with time-crystal physics.

-
- [1] Dominic V. Else, Bela Bauer, and Chetan Nayak, “Floquet time crystals,” *Phys. Rev. Lett.* **117**, 090402 (2016).
- [2] Vedika Khemani, Roderich Moessner, and S. L. Sondhi, “A brief history of time crystals,” (2019), arXiv:1910.10745 [cond-mat.str-el].



Supplementary Figure 1. Time evolution of the spin z -component of (a) the left-most spin and (b) the right-most spin in an $N = 8$ Ising chain, as defined by Eq. 3 above. The initial state is $|\uparrow\uparrow\uparrow\uparrow\uparrow\uparrow\uparrow\uparrow\rangle$. We set $Jt = 0.5$, and allow each spin to include an individual random pulse error within $\pm 20\%$ of the rotation phase. The parameters for magnetic field and coupling noise are the same as in Fig. 2 in the main text. The data are only shown for every 100 Floquet steps.